

Evaluation of Differential Magnification During Brain SPECT Acquisition

Douglass C. Vines and Masanori Ichise

Department of Nuclear Medicine, Mount Sinai Hospital, Toronto and University of Toronto, Toronto, Ontario, Canada

Objective: We developed a modification of the acquisition zoom technique, referred to as differential magnification (DM), to improve the pixel resolution with fanbeam collimators. This study evaluated the effects of DM on brain SPECT image quality.

Methods: SPECT imaging was performed using a triple-head camera with and without DM for a line source in air, Jaszczak and Hoffman phantoms, and 15 clinical patients having regional cerebral blood-flow scans with ^{99m}Tc ECD. Full width at half maximum (FWHM) and contrast ratios were measured on the line source and Jaszczak phantom data, respectively. Visual image evaluation was performed by 2 independent, blinded observers for the Hoffman brain phantom images and clinical patient studies.

Results: FWHM improved on the fanned axis (transverse plane) by 0.05 mm ($P < 0.001$), and the unfanned axis (longitudinal plane) by 0.66 mm ($P < 10^{-6}$), when DM was used. The mean improvement of contrast ratios for the spheres on the Jaszczak phantom with DM was 11.4% ($P < 0.004$). The images with DM were rated superior to those without, for the Hoffman brain phantom and the clinical patients.

Conclusion: This study has demonstrated that SPECT acquisition with fanbeam collimators and DM significantly improves both FWHM and image contrast, resulting in superior image quality. DM techniques may be useful in improving clinical brain SPECT images.

Key Words: brain SPECT; regional cerebral blood flow; fanbeam collimators; differential magnification

J Nucl Med Technol 1999; 27:198–203

SPECT imaging of regional cerebral blood flow (rCBF) has been widely used in the clinical investigation of several neuropsychiatric disorders (1,2). Spatial resolution and sensitivity of photon detection have improved with the development of multihead cameras and fanbeam collimators (FBCs) (3–5). Optimizing all technical aspects of brain SPECT imaging, such

as acquisition and reconstruction, will improve the image quality (6–9).

Acquisition zoom has been used with parallel-hole collimators as a method to improve image resolution and contrast (10–13). This software zoom decreases the pixel size without increasing the matrix size and, therefore, does not require more computer disk space (12,13).

On the other hand, SPECT imaging with FBCs increases sensitivity and improves spatial resolution by introducing magnification along the fanned axis (transverse plane) due to the inherent design of FBCs (14–16). There is no magnification along the unfanned axis (longitudinal plane). The pixel size along the fanned axis is different from that along the unfanned axis and the images before reconstruction are elongated along the fanned axis. A software algorithm during reconstruction (14) corrects this image (pixel) distortion. The net pixel size is equivalent along both axes after reconstruction. To improve the pixel resolution with FBCs, we developed a modification of the acquisition zoom technique referred to as differential magnification (DM). Different magnification factors are applied independently on the fanned and unfanned axes. The image is magnified in the field of view (FOV) along the unfanned axis and magnification also can be applied along the fanned axis. Thus, DM is an acquisition technique used with FBCs to reduce pixel size equally for both axes. The purpose of this study was to implement DM and evaluate its effects on brain SPECT image quality.

MATERIALS AND METHODS

Differential Magnification

The different magnification factors enable the net pixel size to be equal on both axes. The magnification factor used for the unfanned (Y) axis must be larger than that used on the fanned (X) axis to compensate for the inherent magnification of the collimator. DM also is dependent on the radius of rotation (R) of the camera heads. The equation to calculate the unfanned axis magnification, MY, for the system used in this study is (17):

$$MY = (50 + 3)MX / (50 - R), \quad \text{Eq. 1}$$

For correspondence or reprints contact: Douglass C. Vines, BSc, RTNM, Rm. 635, Nuclear Medicine, Dept. of Medical Imaging, Mount Sinai Hospital, 600 University Ave., Toronto, Ontario, Canada M5G 1X5.

where 50 (cm) is the focal length of the collimator, 3 (cm) is the collimator thickness, and MX is the amount of magnification along the X axis.

SPECT Imaging

Four experiments were conducted, each with and without DM, to evaluate the effect of DM. These experiments consisted of SPECT imaging of a line source in air, a water-filled Jaszczak phantom, a Hoffman single-slice brain phantom, and 15 patients. SPECT imaging was performed using a triple-head camera (Prism 3000XP; Picker International, Inc., Cleveland, OH) equipped with an ultra-high resolution FBC and interfaced to a dedicated computer (Odyssey VP; Picker International, Inc., Cleveland, OH). The data were acquired using a continuous scan mode of 3° intervals on a 128 × 128 matrix for 360°, each head rotating 120°.

The capillary line source (1.1- to 1.2-mm internal diameter) first was scanned parallel and then perpendicular to the axis of rotation to measure FWHM along the fanned and unfanned axes of the collimator, respectively. These data were acquired at 10 different R, ranging from 13.4–15.7 cm. The magnification factors for the unfanned axis (MY) were calculated from Equation 1. MX was fixed at 1.33. The data were reconstructed with a ramp backprojection filter. The slices created were 10.15 and 10.87 mm (6 and 5 pixels thick) with and without DM, respectively.

The Jaszczak phantom (model 7000; Data Spectrum Corporation, Chapel Hill, NC) was scanned at an R of 13.5 cm with DM factors 1.33 and 1.93 for the fanned and unfanned axes, respectively. The scan was acquired at a low clinical count level (3 million total counts). The data were reconstructed using a three-dimensional Butterworth postreconstruction filter (order = 5; cutoff frequency = 0.25 cycles/pixel for DM and 0.32 without DM) after applying a ramp backprojection filter. We varied the cutoff frequency (CF) depending on counts per pixel (C) (9,18,19) according to our empirically determined relationship:

$$CF = 0.198 + 3.343 \times 10^{-5} C. \quad \text{Eq. 2}$$

Attenuation correction was performed by assuming uniform attenuation ($\mu = 0.110 \text{ cm}^{-1}$) (20) within a circle drawn around the phantom. The final image slices created were 7.12 and 7.36 mm (2 and 4 pixels) thick without and with DM, respectively, through the sphere segment of the phantom.

The Hoffman phantom (model 8080; Data Spectrum Corporation, Chapel Hill, NC) was placed on the high-resolution parallel-hole collimator and a reference image was obtained for 1 million counts on a 128 × 128 matrix with an acquisition zoom of 2.67. This reference image was used as a standard to which the SPECT images of the phantom were compared (21). SPECT imaging was performed with the phantom positioned so that the long axis of the phantom was parallel to the axis of rotation. This allowed traditional transverse images to be reconstructed parallel to the axis of rotation. The phantom was scanned at 3 clinically relevant count levels including low (3.4), mid (5), and high (6.8) million total counts. R was 12.9 cm. DM factors were 1.33 and 1.89 for the fanned and unfanned axes,

respectively. The data were reconstructed using a three-dimensional Butterworth postreconstruction filter after applying a ramp backprojection filter. At each of the 3 count levels, combinations of 4 orders (1, 5, 9, 13) and 4 CF (0.25, 0.35, 0.45, 0.52) of the Butterworth filter were used. The final images were created at 13.23 mm (6 pixels) thick without and 13.72 mm (8 pixels) thick with DM, respectively. This was to ensure approximately the same thickness as the Hoffman phantom slice (13 mm) to allow comparison of the SPECT image with the standard planar image.

Fifteen patients (7 males, 24–64 y of age; 8 females, 28–73 y of age) with various neuropsychiatric histories were injected with 740 MBq (20 mCi) ^{99m}Tc -ethylcysteinate dimer (ECD; DuPont Merck Pharmaceutical Co., Billerica, MA) and imaged 30 min postinjection with and without DM. Each scan was acquired with an R of 13.5 cm, and the patient remained in the same position for the 2 consecutive scans. The scan sequence in which DM and no DM was performed was varied, so that half the studies were done with DM first and the remaining half without DM first. Scans with DM were performed with the magnification factors fixed at 1.33 and 1.93 for the fanned and unfanned axes, respectively. One-pixel thick transaxial slices from the vertex of the brain to the level of the canthomeatal line were reconstructed using a three-dimensional Butterworth postreconstruction filter (after applying a ramp backprojection filter), order fixed at 5, and CF varied according to C using Equation 2. C was determined by placing an ROI on a summed 120-frame image over the cerebrum. For the initial 5 patients (3 males, 2 females) the scans with DM were acquired with an acquisition time that was 3 times longer than those scans without DM. This yielded approximately the same counts per pixel for both scans (since the pixel size is smaller with DM), and, consequently, the same CF was used. This allowed direct comparison of DM and no DM images with the same filter parameters. The remaining 10 patients were all scanned for the same time, 15 min for both DM and no DM. Attenuation correction was performed by assuming uniform attenuation ($\mu = 0.09 \text{ cm}^{-1}$) within an ellipse drawn around the skull. Images then were reformatted to yield 5-mm thick transoblique slices parallel to the anterior and posterior commissures of the brain (AC-PC line), using a fully automated method of stereotactic image orientation (22). A single image at the level of the midline was selected for each scan with and without DM. These paired images were used for visual image evaluation.

Data Analysis

FWHM in millimeters was measured on 3 different slices and an average was determined for the fanned and unfanned axis with and without DM, respectively. This was done at each of 10 different Rs. Linear regression analysis was used to examine the relationship between FWHM with and without DM and R for the fanned and unfanned axes, respectively. A paired *t* test was performed to compare FWHM with and without DM.

The Jaszczak phantom images of the spheres with and without DM were compared visually and rated for which image best visualized the spheres. Contrast ratios for the spheres also were measured by placing an ROI over the spheres and over

TABLE 1
Mean Differences of FWHM Between Fanned (X)
and Unfanned (Y) Axes

	X	Y
Δ FWHM (mm)*	0.05 ± 0.02	0.66 ± 0.14
Range	0.02–0.09	0.52–0.89
<i>P</i> (paired <i>t</i> -test)	<0.001	< 10^{-6}

*Mean difference between DM and no DM \pm SD.

background to calculate the ratios (23,24). A paired *t* test was performed to compare contrast ratios with and without DM.

The SPECT images of the Hoffman phantom with and without DM were compared visually to the reference standard and evaluated as to which of the pair was better.

The patient images were visually compared between DM and no DM using a set of criteria (9) for 5 anatomical areas. The 5 areas evaluated and the criteria for assessing each image were: (a) anterior cingulate gyrus: 1 (good) = suitable smoothing and separation; 0 (poor) = too smooth or too noisy; (b) basal ganglia (caudate and putamen): 1 = clear contour and homogenous accumulation and separation of caudate and putamen; 0 = too smooth contour or too noisy; (c) internal capsule: 1 = clear visualization; 0 = nonvisualization; (d) thalamus: 1 = clear contour and homogenous accumulation and clear separation of 2 lobes; 0 = too smooth contour or too noisy; (e) right and left visual cortex: 1 = clear separation; 0 = too smooth or unclear separation due to image noise. Scores were summed for each image and compared.

Visual evaluation of images, with and without DM, was performed by 2 independent experienced observers who were blinded to which image was acquired with DM or vice versa.

RESULTS

The mean differences between FWHM with and without DM on both axes, and the results of the paired *t*-test are summarized

in Table 1. On both fanned and unfanned axes, DM demonstrated improvement in FWHM. The mean improvement with DM along the fanned axis was small (0.05 mm) but significant ($P < 0.001$). On the unfanned axis the mean improvement was more substantial (0.66 mm) and significant ($P < 10^{-6}$). The relationship between FWHM with and without DM and R for both axes was linear ($r = 0.88$ – 0.99 , $P < 0.001$) and is shown in Figure 1. The magnitude of improvement of FWHM with DM is similar across R for both the fanned and unfanned axes.

The Jaszczak phantom images demonstrate that DM improves visualization of the spheres (Fig. 2). The mean improvement of the contrast ratios for the spheres with DM was 11.4% ($P < 0.004$). The mean contrast ratio improvement was greatest with the smallest sphere (28%; $P < 0.002$).

The Hoffman phantom images with DM when compared to the standard were preferred to those without DM (Fig. 3).

For the 5 paired clinical patient images with differing acquisition times that had the same filter parameters used for both DM and no DM, DM was judged superior in every case. An example is illustrated in Figure 4A and B. For the remaining 10 paired images (that were both acquired for the same time), DM images were rated higher than those images acquired without it. An example is shown in Figure 4C and D. In 13 of 20 paired images DM was rated higher, there were 2 cases that were equivalent and 5 cases where images without DM were rated higher.

DISCUSSION

The quality of SPECT images is influenced by acquisition parameters as well as those of reconstruction. Thus, the first step in producing high-quality images is to try and optimize the acquisition (6). One parameter of the acquisition to improve is the acquisition matrix size or pixel size. The spatial resolution of a SPECT image is determined by the total system resolution of the camera (intrinsic and collimator resolution), and the size of the image pixels (matrix size) (25). Three-head camera systems are capable of 6-mm resolution (FWHM) in the cortex

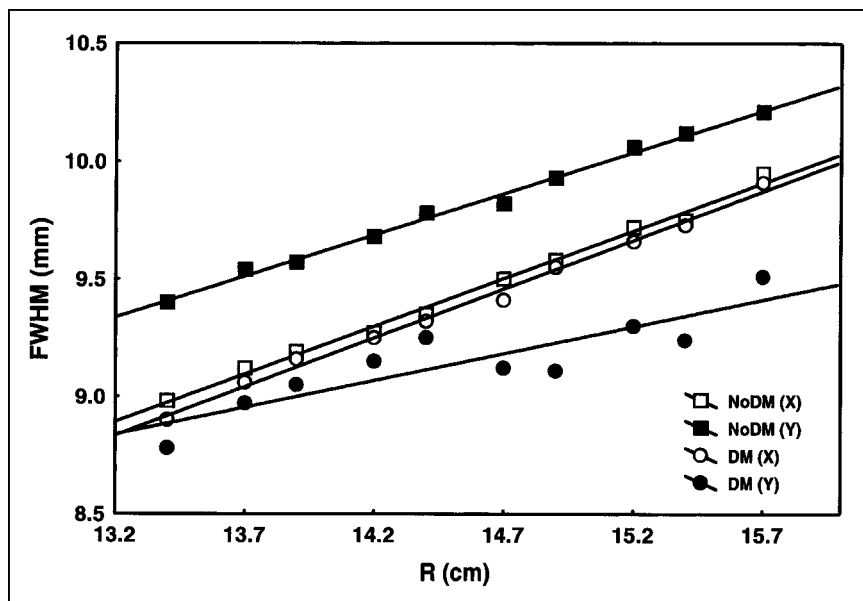


FIGURE 1. The relationship between full width at half maximum (FWHM), with and without differential magnification (DM) and radius of rotation (R), for the fanned and unfanned axes, respectively. Each series was fitted with a linear regression line. X is the fanned axis and Y is the unfanned axis.

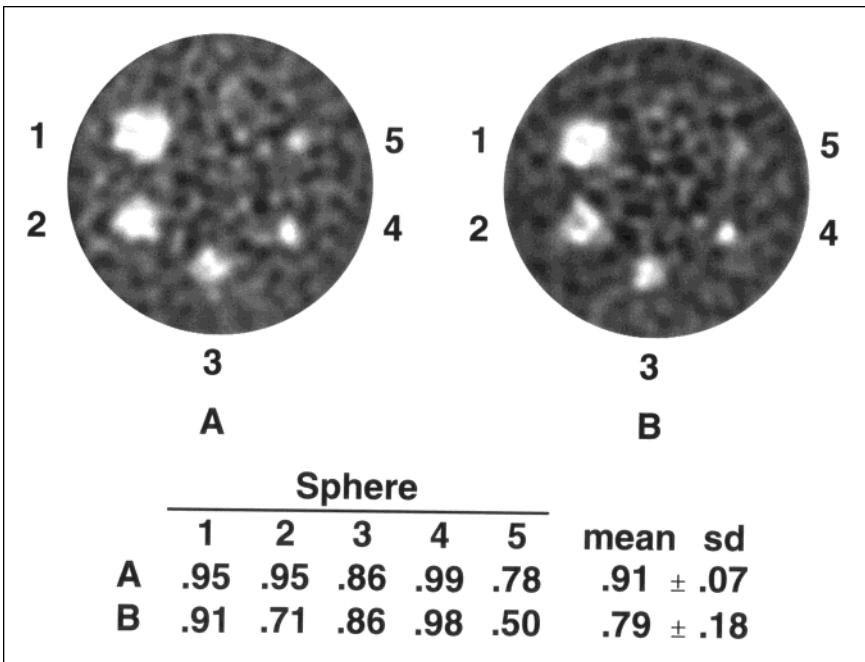


FIGURE 2. SPECT images of the Jaszczak phantom and contrast ratios (A) with differential magnification and (B) without differential magnification.

and 9 mm at the center of the brain, respectively (26). The acquisition pixel size should be less than one third of the FWHM to avoid losing spatial resolution due to the size of the pixels (25), and to ensure adequate sampling and to avoid aliasing artifacts (27). Thus, pixel size should be approximately 2–3 mm. The size of pixels without DM is 3.56 mm. Thus, the 128 matrix size without DM may be limiting the overall resolution. Pixel size on a 256 matrix on the system used is 1.78 mm, and imaging using a 256 matrix would be more appropriate to maximize final image resolution (12). However, doubling

the matrix size requires the acquisition time to be multiplied by a factor of 4 to maintain the same counts per pixel (13). Disk space requirements and processing time also would increase by a factor of 4.

The use of DM in this study reduced the effective pixel size from 3.56–1.84 mm, thus the net effect of using DM is to reduce pixel size in between a 128 and 256 matrix without using more disk space, which would be required on a 256 matrix (13). To maintain the same counts per pixel as an acquisition without DM, the acquisition time with DM was increased by a factor of

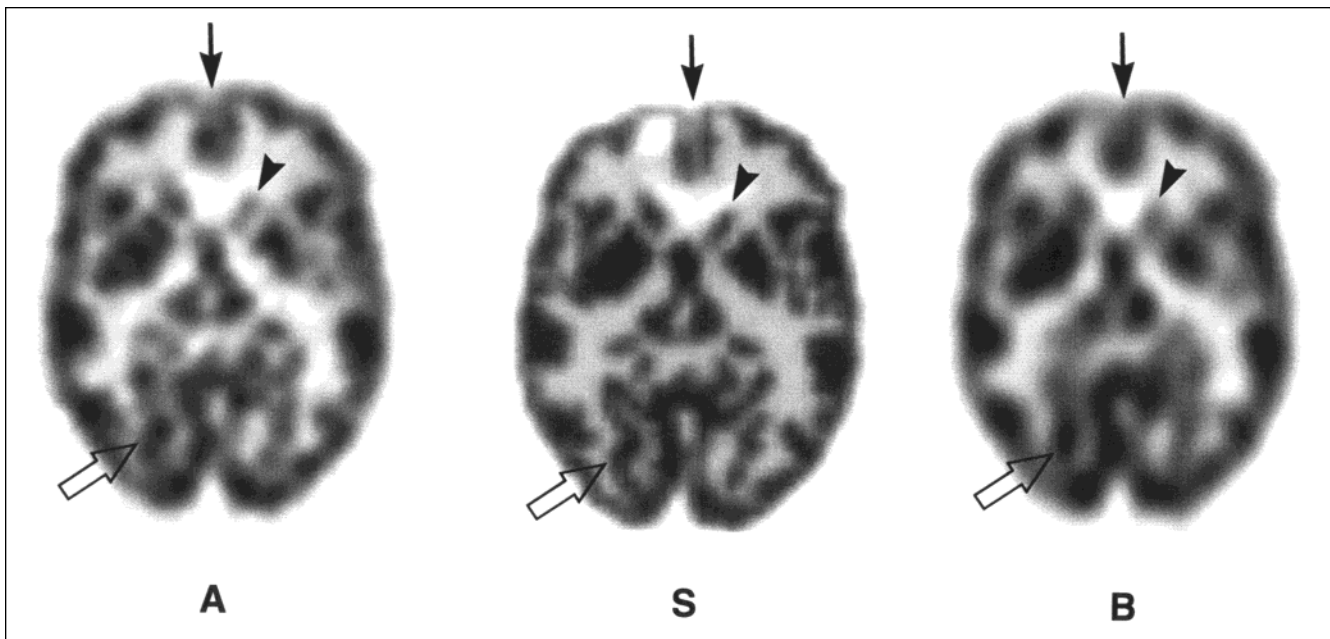


FIGURE 3. SPECT images of the Hoffman single-slice brain phantom at the same count level using the same filter parameters (A) with differential magnification and (B) without differential magnification, compared to the planar standard (S) reference image. Anatomical details of the phantom are more clearly visualized in A than B when compared to S. For example, compare anterior cingulate gyrus (solid arrow), caudate nucleus (arrowhead), and visual cortex (open arrow) between images.

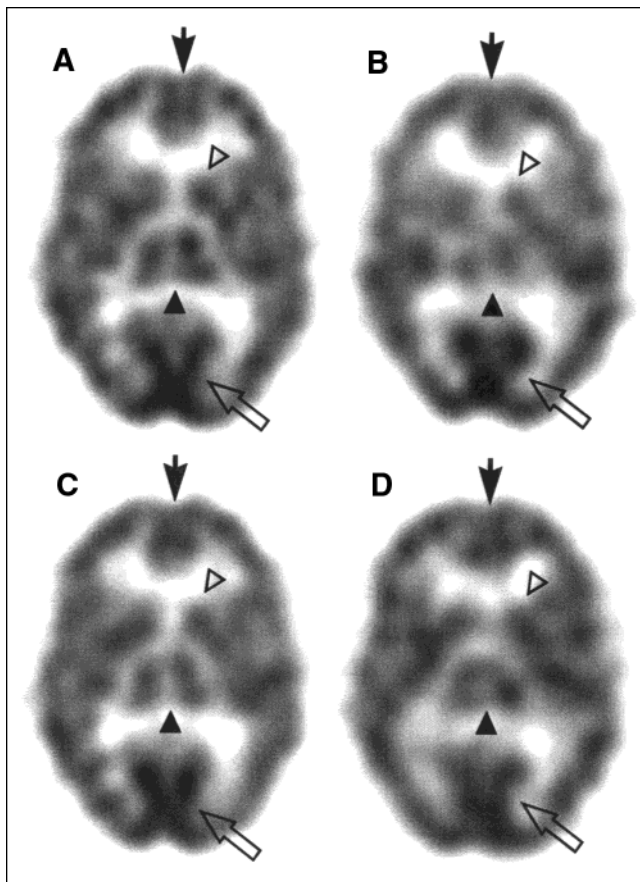


FIGURE 4. Transverse oblique images of a patient acquired (A) with differential magnification and (B) without differential magnification for the same counts per pixel and using the same filter parameters. Image A was rated better than B. Images (C) and (D) without differential magnification were both acquired for the same time. Image C was rated better than D. For example, A and C show a clearer separation of the anterior cingulate gyrus (solid arrow), a more clear contour of the basal ganglia (open arrowhead), separation and more clear contour of the 2 lobes of the thalamus (solid arrowhead), and clearer details of the visual cortex (open arrow).

3. This allowed the same postreconstruction filter to be used, on comparison between DM and no DM it was clearly determined that DM was superior. However, increasing the acquisition time increases the possibility of patient motion, and it may not be practical to increase the acquisition time by a factor of 3. So we evaluated images acquired with and without DM for the same time, using different filters. The results of image evaluation indicate that DM improves image quality without increasing acquisition time. However, there are lower counts per pixel and thus more noise per image (12). A compromise of increasing the acquisition time somewhere in between 1 and 3 times, depending on the patient, may be an appropriate balance to improve image quality without being impractical.

We have demonstrated in this study that FWHM significantly improves with DM along the unfanned axis. The additional improvement on the fanned axis due to DM is very small due to the small magnification factor (1.33) used. The degree to which additional magnification can be applied on the fanned axis is limited by fitting the entire brain into the field of view. This study showed that the overall improvement in FWHM with DM

and the improved image contrast with DM resulted in an observable change in image quality.

There are some limitations with the use of DM. The DM factors vary with R, so each R's unique factors must be determined. This limitation can be simplified by setting R into a few discrete steps with known factors being applied. Second, the use of DM requires precise patient positioning so that no part of the brain is magnified out of the field of view (13). All projections should be checked before beginning the acquisition (28). Finally, the reconstruction filters will be different when using DM because the pixel size is smaller (13). The effects of DM may only be seen if appropriate filters are used. This disadvantage can be overcome by optimizing filter parameters, such as CF, by relating it to counts per pixel and using an objective linear scale.

CONCLUSION

The use of DM significantly improved the FWHM on reconstructed line-source data and image contrast of the Jaszczak phantom. DM also was demonstrated to improve image quality in both phantoms and clinical patient studies, and this can be further improved by increasing the acquisition time. This technique may be useful in improving clinical brain SPECT images.

ACKNOWLEDGMENTS

This work was presented in part at the 43rd Annual Meeting of the Society of Nuclear Medicine, Denver, Colorado, June 3–6, 1996 and was awarded first place for a technologist paper on brain imaging by the Brain Imaging Council. We thank J. Kelly Payne and Michael D. Devous Sr., PhD (University of Texas, Southwestern Medical Center, Dallas, TX) for their helpful suggestions and participation in the visual evaluation of images.

REFERENCES

- Holman BL, Devous MD Sr. Functional brain SPECT: the emergence of a powerful clinical method. *J Nucl Med.* 1992;33:1888–1904.
- Messa C, Fazio F, Costa DC, Ell PJ. Clinical brain radionuclide imaging studies. *Semin Nucl Med.* 1995;25:111–143.
- Fahey FH, Harkness BA, Keyes JW, et al. Sensitivity, resolution and image quality with a multi-head SPECT camera. *J Nucl Med.* 1992;33:1859–1863.
- Links JM. Multidetector single-photon emission tomography: are two (or three or four) heads really better than one? *Eur J Nucl Med.* 1993;20:440–447.
- Kouris K, Costa DC, Jarritt PH, et al. Brain SPECT using a dedicated three-headed camera system. *J Nucl Med Tech.* 1992;20:68–72.
- Juni JE. Taking brain SPECT seriously: reflections on recent clinical reports in The Journal of Nuclear Medicine [Commentary]. *J Nucl Med.* 1994;35:1891–1895.
- Kim HJ, Karp JS, Mozley PD, et al. Simulating technetium-99m cerebral perfusion studies with a three-dimensional Hoffman brain phantom: collimator and filter selection in SPECT neuroimaging. *Ann Nucl Med.* 1996;10:153–160.
- Liu HG, Harris JM, Inampudi CS, Mountz JM. Optimal reconstruction filter parameters for multi-headed brain SPECT: dependence on count activity. *J Nucl Med. Tech.* 1995;23:251–257.
- Minoshima S, Maruno H, Yui N, et al. Optimization of Butterworth filter for brain SPECT imaging. *Ann Nucl Med.* 1993;7:71–77.
- Kouris K, Elgazzar A, Affana R, et al. Methodology and performance assessment of zoom SPECT. *J Nucl Med Tech.* 1990;18:198–203.

11. Early PJ, Mihalic DP. Computer fundamentals. In: Early PJ, Sodee DB, eds. *Principles and Practice of Nuclear Medicine*. 2nd ed. St. Louis, MO: Mosby-Year Book, Inc.; 1995:216–250.
12. Lee K. Nuclear medicine image acquisition methods. In: Lee K, ed. *Computers in Nuclear Medicine: A Practical Approach*. Reston, VA: Society of Nuclear Medicine; 1991:87–98.
13. English RJ. Acquisition parameters, acquisition devices, and the brain. In: English RJ, ed. *SPECT: Single-Photon Emission Computed Tomography: A Primer*. 3rd ed. Reston, VA: Society of Nuclear Medicine; 1995:49–60,83–91,151–163.
14. Tsui BM, Gullberg GT, Edgerton ER, et al. Design and clinical utility of a fanbeam collimator for SPECT imaging of the head. *J Nucl Med*. 1986;27:810–819.
15. Li J, Jaszczak RJ, Turkington TG, et al. An evaluation of lesion detectability with cone-beam, fanbeam and parallel-beam collimation in SPECT by continuous ROC study. *J Nucl Med*. 1994;35:135–140.
16. Tsui BM, Zhao X, Frey EC, McCartney WH. Quantitative single-photon emission computed tomography: basics and clinical considerations. *Semin Nucl Med*. 1994;24:38–95.
17. Tsui BM. Collimator design, properties, and characteristics. In: Simmons GH, ed. *The Scintillation Camera*. Reston, VA: Society of Nuclear Medicine; 1988:17–45.
18. Kotzki PO, Mariano-Goulart D, Quiquere M, et al. Optimum tomographic reconstruction parameters for HMPAO brain SPET imaging: a practical approach based on subjective and objective indexes. *Eur J Nucl Med*. 1995;22:671–677.
19. Taylor D. Filter choice for reconstruction tomography [Editorial]. *Nucl Med Commun*. 1994;15:857–859.
20. Chang LT. A method for attenuation correction in radionuclide computed tomography. *IEEE Trans Nucl Sci*. 1978;NS-25:638–642.
21. Vines DC, Lucas JM, Ichise M, et al. Optimization of brain SPECT filter selection using a brain phantom [Abstract]. *J Nucl Med Tech*. 1993;21:108.
22. Tsao J, Stundzia A, Ichise M. Fully automated establishment of stereotaxic image orientation in six degrees of freedom for technetium-99m-ECD brain SPECT. *J Nucl Med*. 1998;39:503–508.
23. Heller SL, Goodwin PN. SPECT instrumentation: performance, lesion detection, and recent innovations. *Semin Nucl Med*. 1987;17:184–199.
24. Rosenthal MS, Cullom J, Hawkins W, et al. Quantitative SPECT imaging: a review and recommendations by the Focus Committee of the Society of Nuclear Medicine Computer and Instrumentation Council. *J Nucl Med*. 1995;36:1489–1513.
25. Sorenson JA. Nuclear medicine tomography: principles, and digital image processing in nuclear medicine. In: Sorenson JA, Phelps ME, eds. *Physics in Nuclear Medicine*. 2nd ed. Philadelphia, PA: WB Saunders Co.; 1987:391–423,452–464.
26. Devous MD Sr. Instrumentation, radiopharmaceuticals, and technical factors. In: Van Heertum RL, Tikofsky RS, eds. *Cerebral SPECT Imaging*. 2nd ed. New York, NY: Raven Press; 1995:3–19.
27. Huang SC, Hoffman EJ, Phelps ME, Kuhl DE. Quantitation in positron emission computed tomography: 3. effect of sampling. *J Comput Assist Tomogr*. 1980;4:819–826.
28. Croft BY. Instrumentation and computers for brain single photon emission computed tomography. *Semin Nucl Med*. 1990;20:281–289.